Systematics of the Induced Magnetic Moments in 5*d* Layers and the Violation of the Third Hund's Rule

F. Wilhelm,* P. Poulopoulos,† H. Wende, A. Scherz, and K. Baberschke
Institut für Experimentalphysik, Freie Universität Berlin, Arnimallee 14, D-14195 Berlin-Dahlem, Germany

M. Angelakeris and N. K. Flevaris
Department of Physics, Aristotle University of Thessaloniki, 54006 Thessaloniki, Greece

A. Rogalev
European Synchrotron Radiation Facility (ESRF), BP 220, 38043 Grenoble, France
(Received 25 April 2001; published 25 October 2001)

X-ray magnetic circular dichroism measurements are reported at the beginning (W) and at the end (Ir, Pt) of the 5*d* series of the periodic table. Considerable induced magnetic moments of about 0.2 μ_B/atom were probed for the nonmagnetic W and Ir and compared to previous data for the Pt induced moments in multilayers. W was found to couple antiferromagnetically and Ir ferromagnetically to the 3*d* layers. Finally, the W spin and orbital magnetic moment couple in parallel, contrary to what is expected from the third Hund's rule. This remarkable finding shows that the induced magnetic behavior of 5*d* layers may be radically different than that of impurities and alloys.

DOI: 10.1103/PhysRevLett.87.207202 PACS numbers: 75.70.Cn, 75.70.–i, 78.70.Dm

Interface magnetism is dominated by local structural and electronic modifications with respect to the bulk, and it is of some importance to understand the magnetic properties of ultrathin multilayer structures. The magnetic polarization of the nonmagnetic transition metal (TM) layers is one of these modifications. It contributes significantly, for example, to the enhanced magneto-optic response [1] and spin-dependent scattering that governs magnetotransport properties [2]. Recently, it was suggested that for the 3*d* series of the periodic table interface magnetic moments may be well estimated by data of the corresponding binary bulk alloys and the coordination number [3]. However, in alloys or as impurities, the nonmagnetic atoms are coupled mainly to ferromagnetic (FM) nearest neighbors. In a multilayer, on the other hand, two-dimensional directly coupled nonmagnetic layers are formed facing a FM layer. In the present work we demonstrate through a systematic investigation of 5*d* layers that the induced magnetism in layered structures may be radically different than that of impurities and alloys due to the different geometry and electronic structure.

Actually, besides Pt [4–6] the induced magnetic moments of 5*d* elements in multilayers are unexplored. Only now, the progress of techniques with element specificity and monolayer sensitivity like the x-ray magnetic circular dichroism (XMCD) [7] and the realization of third generation synchrotron radiation facilities working in the hard x-ray regime opens the road for a systematic study of the induced magnetism in thin multilayer structures. In this Letter we report on the induced magnetic moments at the W and Ir layers in their multilayers with Fe. Magnetic polarization of W and Ir impurities in a magnetic environment was previously detected [8,9]. However, this is the first experimental determination, to our knowledge, of induced magnetic moments of W and Ir at interfaces with 3*d* FM layers, where up to now only results from *first principle* calculations on some interface orientations are available [10–12]. We probe considerable induced magnetic moments of about $0.2\mu_B$ per atom for W and Ir. The Ir magnetic moment is polarized in parallel to Fe, while the Ir spin μ_S and orbital μ_L moments are coupled in parallel to each other, as one expects for a TM with a more-than-half-filled 5*d* shell. For the less-than-half-filled 5*d* shell TM W, on the other hand, the induced magnetic moment is antiparallel to the Fe moment. However, μ_S and μ_L couple in parallel, contrary to what is predicted by the third rule of Hund. It is surprising that Hund's rules which were developed in an atomistic picture hold so well for solids, too. No violation of the third Hund's rule was addressed by experiments [13].

Fe/W and Fe/Ir multilayers were grown by *e*-beam evaporation on Kapton under ultrahigh vacuum conditions. Kapton is ideal for XMCD measurements because of its small background signal. Moreover, it was shown not to deteriorate the structural and magnetic properties of the samples with respect to glass or Si substrates [14]. Structural characterization by x-ray diffraction and transmission electron microscopy revealed polycrystalline multilayer morphology with bcc(001) texture. The sample quality was supported by magnetic measurements via vibrating sample magnetometry. The XMCD experiments were performed at the European Synchrotron Radiation Facility in Grenoble (France) on the ID12A beam line [15] at the W and Ir $L_{2,3}$ edges using the fluorescence yield detection mode. The degree of polarization of the circular light was 84%. Large magnetic fields of 5 T were applied normal to the film plane and along the x-ray beam direction for complete magnetic saturation at a

temperature of 10 K. The XMCD spectra were recorded either by changing the helicity of the light or by inverting the direction of the magnetic field. The determination of the magnetic moments for W and Ir was done by application of the sum rules [16].

In Figs. 1 and 2 we see normalized x-ray absorption (XAS) and XMCD spectra at the $L_{3,2}$ edges of W in Fe/W and Ir in Fe/Ir multilayers, respectively. The total Fe thickness in each multilayer period is 1.0(1) nm, while the W, Ir thicknesses are 0.5(1) nm. The thickness of the nonmagnetic element corresponds to about only 3.0(5) monolayers in order to ensure that the major amount of it is found at the interface with Fe. For the XAS spectra the ratio of the L_3/L_2 was normalized to 2.19/1 and 2.24/1 for W and Ir, respectively, according to [17]. The existence of finite XMCD signals shows that both elements have acquired induced magnetic moments. The XMCD signals are very small with respect to the XAS, as the large scaling factors of 50 (Fig. 1) and 20 (Fig. 2) reveal. However, the signal-to-noise ratios of the XMCD are still large. At this point, we have to stress the high quality of our XMCD spectra with respect to previous ones for the W and Ir as impurities in a bulk Fe matrix [8]. This quality is related to the high photon flux and degree of polarization offered by the third generation synchrotron radiation facilities [15].

One may notice the different sign of the XMCD spectra at the corresponding edges showing that the two elements are coupled in an opposite direction with respect to Fe. By knowing the direction of the magnetic field and the helicity of the beam we conclude that W is polarized antiparallel and Ir parallel to Fe, in agreement with previous reports for the impurities [8]. This behavior originates from a general trend in all TM series with the $5d$ band filling. For an approximate interpretation one can regard the well-known Bethe-Slater curve: the ratio of the interatomic distances to the radii of the incompletely filled d shells decreases by moving from the larger to the lower filling and it leads to a change of the sign of the exchange integral J from positive (FM) to negative [antiferromagnetic (AFM)]. Recent rigorous calculations suggest that the hybridization between the $3d$-$5d$ bands changes the relative position of the majority and minority bands with respect to the Fermi energy and they provide the sign of the induced moment [18]. In our case, Ir has a more-than-half-filled $5d$ shell and, therefore, positive J, while W is less than half filled and has a negative J.

Here we focus on the different shape of W and Ir XMCD signals. The Ir ones are simple and similar to Pt [6]. The maxima of XAS and XMCD in such spectra coincide. On the other hand, the W XMCD maximum is found slightly on the left of the edge. The asymmetry at L_3 (similarly at L_2), which is marked by an arrow, is for the first time resolved for W. The origin of such asymmetries has been discussed recently with respect to the spin polarization [19]. Our XMCD spectra are in remarkable agreement to spectra calculated by recent full-relativistic first principles calculations, though the latter concerned a different geometry

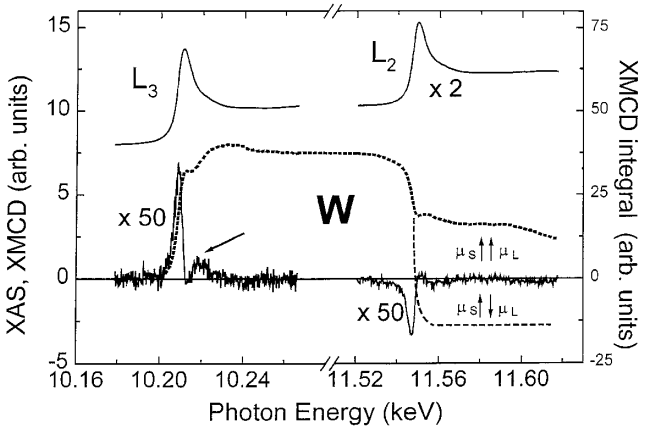

FIG. 1. Normalized XAS (top) and XMCD (bottom) spectra measured at the $L_{3,2}$ edges of W in a Fe/W multilayer. For better illustration the XMCD spectra have been multiplied by 50, while the XAS spectra have been vertically shifted. The XMCD integrals (dotted line: measured; dashed line: hypothetical) serve to visualize the relative orientation of μ_L and μ_S. For the arrow, see the text.

[11]. To deduce the magnetic moments one applies a set of rules known as the "sum rules" [16]. In the final relations the integrated intensities under the XMCD spectra and the "white line" intensities, which are proportional to the number n_h of the d holes, appear. For W and Ir it is simple to calculate the XMCD intensities because the edges are well separated. For the white line intensities, one usually subtracts the continuum from the XAS. The continuum is artificially represented by a step function, and this recipe has been extensively applied for the $3d$ FM metals; however, its validity has been recently questioned [20]. An alternative approach has been applied in cases where the white line intensity is rather small, as in $4d$ elements Pd [21] and $5d$ Pt [22,23]. In this method a relative comparison between the XAS of Ag and Pd or Au and Pt allows for the determination of n_h [21]. In Fig. 3 we plot the XAS spectra at the L_2 edge of W, Ir, and Pt. Moreover, we

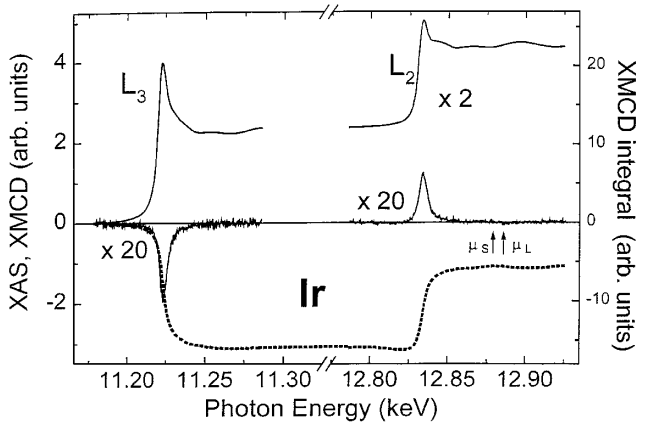

FIG. 2. Normalized XAS (top) and XMCD (bottom) spectra measured at the $L_{3,2}$ edges of Ir in a Fe/Ir multilayer. For better illustration the XMCD spectra have been multiplied by 20. The XMCD integrals serve to visualize the relative orientation of μ_L and μ_S.

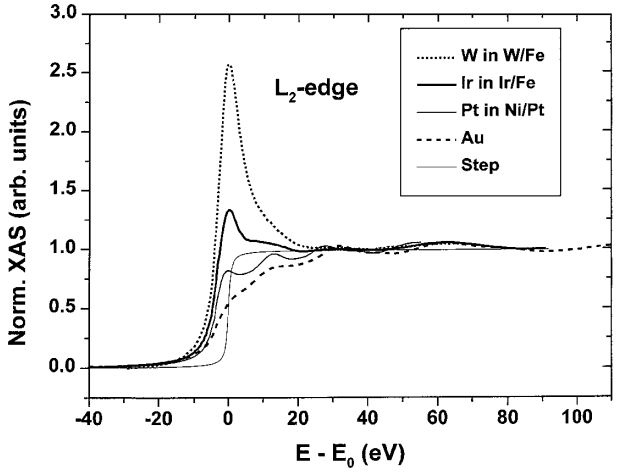

FIG. 3. XAS spectra for W, Ir, Pt, and Au at the L_2 edge. The spectra are horizontally shifted as it is explained in the text. A step function that represents the continuum is also shown.

plot the corresponding Au XAS and a step function. To compare the various spectra, these have been shifted horizontally and their maximum has been brought to the zero of the energy axis.

First we discuss the method of using the Au spectra for n_h. The energy scale of the Au spectra has been stretched to match the W and Ir spectra as described in [22] in order to evaluate n_h. This is certainly an approximation, since the Au fcc structure is different than the W and Ir bcc. However, one sees that we can match the extended x-ray-absorption fine structure wiggles between these elements. For the theoretical values of n_h we used the results of first principles calculations yielding 2.7 holes for Ir and 5.7 holes for W [24]. For Au we took $n_h = 0.74$ [22]. Using the same approach to the spectra at the L_3 edges and combining the numbers with the L_2 ones through the sum rules, we deduce the spin μ_S and orbital μ_L contributions and the total magnetic moment μ_{tot} (Table I). Now, we turn to the use of the step function. Clearly, it cannot work for Pt, supporting the ideas of [21]. However, Ir and W have relatively large white line intensities and one can apply the step-function method. The results of this approach are also included in Table I. By comparing the two approaches one sees that they work well for W (within 6%) and moderately for Ir (15%) exactly because Ir has a smaller white line intensity than W.

Table I can be used as a starting point to discuss the induced magnetic moments at the interfaces of the $5d$ elements. W and Ir carry a total magnetic moment of about $0.2\mu_B$ per atom. This has to be compared to the $0.3\mu_B$ per atom for Pt (Table I) detected at similarly prepared samples with very thin Pt layers and thicker Ni ones [6,23] or the $0.5\mu_B$ per atom for Pt in Fe/Pt multilayers prepared by sputtering methods [5]. Recent theoretical works report for W at a single interface with 1–2 ML of Fe spin moments of about $-0.1\mu_B$ per atom [10,11]. On the other hand, experiment and calculations for the W impurities give much larger values of about $-0.4\mu_B$ per atom [8]. Our $-0.2\mu_B$ per atom is, consequently, in good agreement with the calculations for W layers [10,11] by considering the larger polarization coming from the two interfaces of W with Fe. For Ir, calculations for impurities in a Fe matrix predict $+0.3\mu_B$ to $+0.4\mu_B$ per atom [8]. First principles calculations for Fe_5/Ir_3 superlattices report for Ir a magnetic moment of about $+0.2\mu_B$ per atom [12], in excellent agreement with our measurements.

TABLE I. Data for the induced magnetic moments for three $5d$ elements (W, Ir, and Pt) of the periodic table. For W and Ir the results yielded by the Au and the step-function approach are compared. The results for Pt have been taken from a multilayer with 1.2 nm Ni and 0.4 nm Pt [6,23]. The absolute error bars are 15%. For Ir the maximum contribution comes from the method of analysis of the white line, while for W it comes from the more complicated shape of the XMCD spectra.

	$\mu_S(\mu_B/\text{atom})$	$\mu_L(\mu_B/\text{atom})$	$\mu_{\text{tot}}(\mu_B/\text{atom})$
W Au-approach	−0.17	−0.015	−0.19
W step-function	−0.18	−0.016	−0.20
Ir Au-approach	0.17	0.016	0.18
Ir step-function	0.20	0.019	0.21
Pt Au-approach	0.24	0.056	0.29

A second important point of Table I to be discussed is the ratio μ_L/μ_S. This ratio has the advantage not to be influenced by the use of a step function. For Pt we have reported ratios of about 0.2–0.3. Here, we see that the ratio for Ir is about only 0.1. This may be understood by the fact that Ir is before Pt in the periodic table and, therefore, it is expected to have reduced μ_L/μ_S, i.e., reduced contribution of the orbital magnetism, as, for example, occurs by going from Ni to Co and Fe. Our number is well compared to the one of 0.12 reported for Ir in $Cr_{0.975}Ir_{0.025}O_2$ [9]. For W we find $\mu_L/\mu_S = 0.09$, which is slightly smaller compared to the 0.1–0.2 reported by first principles calculation [11].

Finally, we question if the third Hund's rule holds for the $5d$ layers. Recent first principles theoretical calculations [10,11] for Fe/W(110) interfaces report that $\mu_L/\mu_S > 0$ without, unfortunately, any discussion with respect to the Hund's rules. An older reference [8(b)] provides experimental and theoretical values for $5d$ impurities in Fe where one may see that for Os, Re, and Ir the third Hund's rule should not hold; however, this problem was not addressed at all. For W impurities μ_L and μ_S were antiparallel [8(b)]. Our experiment, though performed at the Fe/W(001) geometry, is in agreement with [10,11] that for W layers $\mu_L/\mu_S > 0$. This is visualized with the help of the XMCD integrals in Fig. 1. The measured integral (dotted line) is not changing sign exactly as in the case of Ir (Fig. 2) showing that $\mu_L/\mu_S > 0$. For a negative sign the XMCD integrals should change sign as the hypothetical dashed line of Fig. 1 reveals. The opposite signs of μ_L/μ_S for W in alloys [8(b)] and multilayers show that induced magnetism in layers might be radically different than in alloys.

The positive μ_L/μ_S for W is surprising because W has a less-than-half-filled $5d$ shell and according to Hund's rules in an atomistic picture one would expect a negative sign. According to recent first principles calculations the intermetallic compounds VAu_4 and VPt_3 are candidates to violate the third Hund's rule and the effect is attributed to the influence of ligand states [13]. The hybridization between the V and Au (or Pt) d states and the large spin-orbit coupling of Au (or Pt) are predicted to reverse the sign of μ_L for V. In other words, there are terms in the Hamiltonian where the intra-atomic spin-orbit coupling at the one site affects the total orbital moment at another site (because the actual wave function is delocalized). This was nicely demonstrated in [13] by turning on (off) the spin-orbit coupling at the Au site and observing a parallel (antiparallel) configuration of μ_S and μ_L at the V site. Although [13] provides some insight within theory, no experimental confirmation exists up to now. Interestingly, in our case the larger spin-orbit coupling is exhibited by W and not by Fe. To illustrate our ideas in a simplified atomistic picture we may consider the following three types of interaction between the spin S_z and orbital angular momentum L_z projections: (i) $J_{\text{inter}} S_z^{\text{Fe}} S_z^{\text{W}}$, (ii) $\lambda_{\text{intra}}^{\text{W}} S_z^{\text{W}} L_z^{\text{W}}$, and (iii) $\lambda_{\text{inter}} S_z^{\text{Fe}} L_z^{\text{W}}$ (J, λ are constants). The first (interatomic exchange) favors, as discussed before, the AFM coupling between Fe and W. The second one is an intra-atomic spin-orbit interaction for W which should obey, in principle, the third Hund's rule. In order for S_z^{W} and L_z^{W} to be FM coupled, as the experiment reveals, the third (interatomic spin-orbit) interaction should favor AFM coupling between S_z^{Fe} and L_z^{W} *and* it has to be stronger than the second interaction. The fact that the first principles theoretical calculations [10,11] predict also a FM coupling between S_z^{W} and L_z^{W} suggests that indeed this condition is realized through hybridization between Fe and W. The role of such interatomic spin-orbit interactions was also recognized in the past for a better description of the properties of many electron systems [25,26].

In summary, by virtue of the element-specific XMCD we probe directly the induced spin and orbital magnetic moments of three $5d$ elements, namely, W, Ir, and Pt. The interplay of the spin moment of Fe and the spin and orbital moments of the $5d$ layers produces unexpected results. It is the competition between intra-atomic spin-orbit coupling in W and the interatomic spin-orbit coupling between the S_z^{Fe} and L_z^{W} in combination with the leading exchange coupling $J_{\text{inter}} S_z^{\text{Fe}} S_z^{\text{W}}$, which results in a parallel alignment between the W spin and orbital moments. This looks like a violation of the third Hund's rule. In a solid it should not be surprising that a stronger interatomic spin-orbit coupling at an interface may lead to a coupling which is not expected in an atomic picture. However, here we discuss first experimental evidences.

We thank K. H. Bennemann and O. Eriksson for illuminating discussions. The work was supported by the BMBF (05 SC8 KEA3, 05 KS1 KEB 4), by the DFG (Sfb290 TPA2), and by the ESRF (HE-636 experiment). Samples were prepared within projects supported by the GSRT.

Note added.—B. Johansson brought to our attention a different case of breakdown of Hund's third rule. By applying an external field in uranium metals **L** and **S** are theoretically predicted to be parallel aligned [27].

*Present address: European Synchrotron Radiation Facility (ESRF), BP 220, 38043 Grenoble, France.
†Corresponding author.
Email address: babgroup@physik.fu-berlin.de

[1] E. R. Moog *et al.,* J. Appl. Phys. **69**, 4559 (1991).
[2] R. Coehoorn, J. Magn. Magn. Mater. **151**, 341 (1995).
[3] A. M. Niklasson *et al.,* Phys. Rev. B **59**, 6373 (1999).
[4] G. Schütz *et al.,* J. Appl. Phys. **73**, 6430 (1993).
[5] W. J. Antel, Jr. *et al.,* Phys. Rev. B **60**, 12 933 (1999).
[6] F. Wilhelm *et al.,* Phys. Rev. Lett. **85**, 413 (2000).
[7] *Spin-Orbit-Influenced Spectroscopies of Magnetic Solids, Proceedings of an International Workshop, Herrsching, Germany, 1995,* edited by H. Ebert and G. Schütz, Lecture Notes in Physics Vol. 466 (Springer, Berlin, New York, 1996), and references therein; H. Ebert, *ibid.,* pp. 159–177.
[8] (a) R. Wienke *et al.,* J. Appl. Phys. **69**, 6147 (1991); (b) G. Schütz *et al.,* Phys. Scr. **T49**, 302 (1993).
[9] P. Dalmas de Réotier *et al.,* J. Phys. (Paris), Colloq. **7**, C2-453 (1997).
[10] X. Qian and W. Hübner, Phys. Rev. B **60**, 16 192 (1999); **64**, 092402 (2001).
[11] I. Galanakis *et al.,* Phys. Rev. B **62**, 3923 (2000).
[12] D. Stoeffler, in *Ferienkurse des Instituts für Festkörperforschung 1999, "Magnetische Schichtsysteme"* (Forschungszentrum Jülich, Jülich, 1999), Vol. 30, Sec. B.4.1.
[13] I. Galanakis *et al.,* Phys. Rev. B **63**, 172 405 (2001); I. Galanakis *et al.,* J. Phys. Condens. Matter **13**, 4553 (2001).
[14] M. Angelakeris *et al.,* J. Appl. Phys. **82**, 5640 (1997).
[15] J. Goulon *et al.,* Physica (Amsterdam) **208B&209B**, 199 (1995).
[16] B. T. Thole *et al.,* Phys. Rev. Lett. **68**, 1943 (1992); P. Carra *et al., ibid.* **70**, 694 (1993).
[17] B. L. Henke, E. M. Gullikson, and J. C. Davis, At. Data Nucl. Data Tables **54**, 181–342 (1993); see, for example, www-cxro.lbl.gov.
[18] H. Yamada and M. Shimizu, J. Phys. F **15**, L175 (1985); M. S. S. Brooks *et al.,* J. Phys. Condens. Matter **1**, 5861 (1989).
[19] G. van der Laan, J. Phys. Condens. Matter **9**, L259 (1997); Phys. Rev. B **55**, 8086 (1997).
[20] A. L. Ankudinov *et al.,* J. Synchrotron Rad. **8**, 92 (2001).
[21] J. Vogel *et al.,* Phys. Rev. B **55**, 3663 (1997).
[22] W. Grange *et al.,* Phys. Rev. B **58**, 6298 (1998).
[23] P. Poulopoulos *et al.,* J. Appl. Phys. **89**, 3874 (2001).
[24] V. Popescu and H. Ebert (private communication).
[25] A. Fert and P. M. Levy, Phys. Rev. Lett. **23**, 1538 (1980); P. M. Levy *et al.,* J. Appl. Phys. **53**, 2168 (1982).
[26] A. K. Rajagopal and M. Mochena, Phys. Rev. B **57**, 11 582 (1998).
[27] A. Hjelm *et al.,* Phys. Rev. Lett. **71**, 1459 (1993).